THE JOURNAL OF PHYSICAL CHEMISTRY C
A JOURNAL OF THE AMERICAN CHEMICAL SOCIETY

pubs.acs.org/JPCC

Article

Tunable Couplings of Photons with Bright and Dark Excitons in Monolayer Semiconductors on Plasmonic-Nanosphere-on-Mirror Cavities

Jie Fang,[⊥] Suichu Huang,[⊥] Kan Yao,[⊥] Tianyi Zhang, Mauricio Terrones, Wentao Huang, Yunlu Pan, and Yuebing Zheng*

Cite This: J. Phys. Chem. C 2023, 127, 9105−9112

Read Online

ABSTRACT: Tunable exciton−photon couplings are of great importance for cavity quantum electrodynamics (QED), polariton chemistry, optical computing, and bosonic lasing. In this regard, two-dimensional (2D) excitons in transition metal dichalcogenides (TMDs) have attracted tremendous interest—the huge oscillator strengths endow sensitive responses to optical modes, and their excitonic properties can be actively tuned by external stimuli. However, tunable coupling with spin-forbidden dark excitons in monolayer TMDs has rarely been demonstrated, and how the bright/dark-exciton−photon couplings coexist in one system is still a mystery. Herein, we utilize waveguide and antenna modes in a gold nanosphere-on-mirror cavity to match the in-plane and out-of-plane dipole moments of bright and dark excitons in monolayer WS_2, respectively, and simultaneously. Strong bright-exciton−photon couplings with a coupling strength of up to 60 meV are observed at room temperature. We show that the waveguide mode can be tuned in wavelengths by controlling the spacer thickness and demonstrate the anti-crossing feature of polaritons. Next, by increasing the excitation angle, we dynamically enlarge the relative contribution from the antenna mode coupled with dark excitons and suppress the waveguide mode coupled with bright states. Moreover, a tunable bright exciton linewidth is achieved as a result of suppressed homogeneous broadening caused by the dominant dark exciton decays under strong dark-exciton−photon couplings. This is not only proof of tunable couplings with dark excitons but also an insightful finding that reveals the novel interactions between bright- and dark-exciton−photon hybrids in a single optical cavity, opening new possibilities in tunable QED.

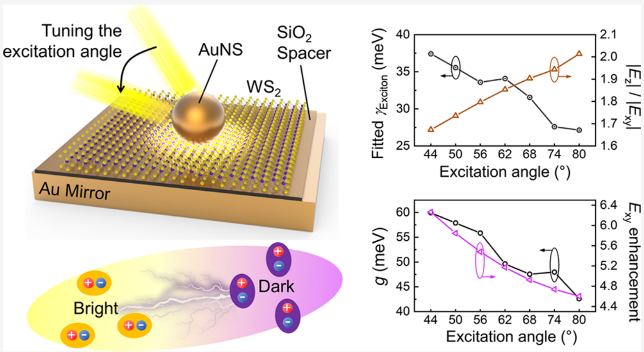

■ INTRODUCTION

Monolayer transition metal dichalcogenides (TMDs), possessing direct band gaps, strong exciton binding energies, high carrier mobilities, and robust mechanical properties, have attracted great research interests.[1−5] The fruitful excitonic complexes with large oscillator strengths in monolayer TMDs make them a fascinating platform for studying cavity quantum electrodynamics (QED) at room temperature.[6−9] One of the most attractive topics in QED is the tunable exciton−photon coupling, which has opened up tremendous prospects in polariton chemistry engineering,[10] photon quantum computing,[11] and tunable optical devices.[12] Therefore, over the past decades, lots of efforts have been made in developing tunable couplings with the two-dimensional (2D) excitons in TMDs. For example, through electrical gating[13−15] or adjusting the dielectric environment,[16,17] people have tuned TMD-based QED systems by manipulating the intrinsic properties of bright excitons. In addition, a tunable optical cavity mode is also an effective approach for controllable exciton−photon couplings. Dufferwiel et al. employed two dielectric-distributed Bragg reflectors with nanopositioners to form a separation-adjustable Fabry−Pérot cavity for tunable couplings with bright excitons in TMDs.[18] Kleemann et al. introduced different spacer thicknesses in a nanosphere-on-mirror (NSoM) cavity by coupling it with WSe_2 flakes of different numbers of layers and demonstrated a tunable strong coupling (SC).[19]

Recently, besides the commonly studied bright excitons, the spin-forbidden excitonic states in monolayer TMDs, i.e., dark excitons,[20] have also aroused new attention in cavity QED.[21−23] Dark excitons are promising for quantum computing and Bose−Einstein condensation because of their long lifetimes, but meanwhile, they are optically inactive at

Received: February 14, 2023
Revised: April 22, 2023
Published: May 5, 2023

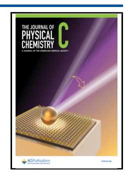

https://doi.org/10.1021/acs.jpcc.3c01019
J. Phys. Chem. C 2023, 127, 9105−9112

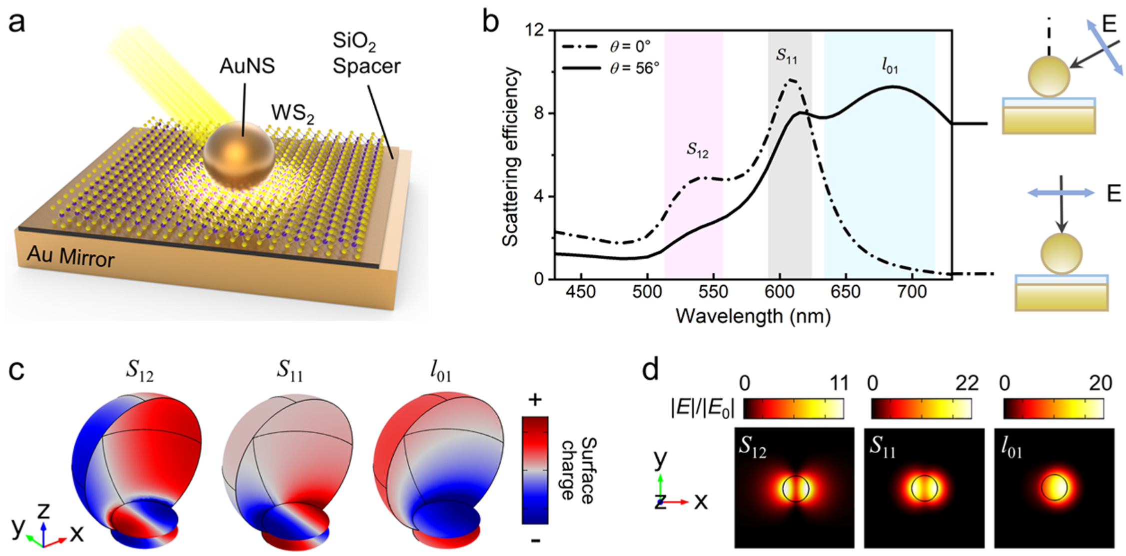

Figure 1. (a) Schematic of the system in the study, in which monolayer WS_2 is coupled to a 100 nm AuNS on a mirror cavity with a 7−14 nm SiO_2 spacer. (b) Simulated excitation-angle (θ)-dependent total scattering efficiency of such a NSoM cavity, where the spacer thickness is 9 nm, and the excitation light is TM-polarized, as shown in the schematics. The pink, gray, and blue shaded areas label the three cavity modes S_{12}, S_{11}, and l_{01}, respectively. (c, d) Characterization of different cavity modes. Simulated (c) surface charge and (d) E-field enhancement when $\theta = 0°$ for S_{12} mode and when $\theta = 56°$ for S_{11} and l_{01} modes. The black contours in panel (c) highlight half of the sphere's surface, the facet of the sphere at the spacer's top surface, and its projection at the bottom surface. The black circles in panel (d) denote the interface between the sphere and the spacer.

room temperature and thus hard to harness. Coupling dark excitons with the cavity photons can dramatically boost their exciton decay rates, enabling the all-optical read-out and control.[22,23] However, tunable coupling with dark excitons in monolayer TMDs has rarely been demonstrated, which limits the development of functional devices based on such dark states. Moreover, the strong many-body effects in monolayer TMDs determine a close interaction between the bright and dark states, significantly affecting each other's excitonic quantum dynamics.[24] Several groups have reported the dark exciton-mediated phenomena in strongly coupled bright excitons−photon hybrids.[24−26] Latini et al. have even theoretically predicted the mixing of bright and dark excitons spectral features when they are both strongly coupled in a QED system,[27] but an experimental study is still demanded. Therefore, simultaneously coupling bright and dark excitons in a single system could potentially bring new insights into fundamental physics, and if further achieved in a tunable manner, stupendous opportunities would be opened up. This motivates the search for applicable optical cavities with novel tunability.

Plasmonic NSoM cavities are made of a metallic nanosphere standing on a dielectric-coated mirror, which support highly confined light field down to deep-subwavelength scales in the gap between the nanosphere and mirror.[28−31] The complex hybridization of plasmons in such a configuration leads to various cavity modes,[32−38] providing more degrees of freedom in design to match the in-plane and out-of-plane dipole moments of bright and dark excitons in monolayer TMDs.[39−41] Moreover, in comparison with other nano-particle-on-mirror counterparts such as structures based on nanocubes or nanowires, nanosphere-based cavities can generate an extremely excitation-sensitive out-of-plane antenna mode in contrast to the in-plane waveguide modes because of their unique morphology and symmetry.[36,38] This makes NSoM a good candidate for us to design tunable couplings with dark excitons as well as the dynamic interaction between bright- and dark-exciton−photon hybrids.

In this work, we report the experimental demonstration of tunable couplings with bright and dark excitons in monolayer WS_2 in a single gold NSoM cavity at room temperature. With a rational design of the cavity, enhanced in-plane and out-of-plane E-fields confined at the WS_2 position are generated at the wavelengths of bright and dark excitons respectively and simultaneously. By adjusting the spacer thickness, a clear anti-crossing feature of polaritons is observed in the scattering spectra at the bright exciton energy, revealing the SC nature. Coupled-mode-theory (CMT) fittings confirm a coupling strength of up to 60 meV. Moreover, by changing the excitation angle, dynamic control of the coupling strength with bright excitons is achieved, and a tunable coupling with dark excitons is demonstrated, evidenced by the modulation on the coherent linewidth of bright excitons from 37.5 down to 27.1 meV. The narrowed linewidth is attributed to the suppressed homogeneous broadening caused by the dominant dark state decays under strong dark-exciton−photon couplings, shedding light on the mystery of multiparticle interactions in TMD-based QED. Our findings would bring up new possibilities in tunable photonic devices, cavity chemistry, and optical computing.

■ METHODS

Preparation of Monolayer WS_2. Monolayer WS_2 is synthesized inside a 1 in. quartz tube furnace by an alkali metal halide-assisted chemical vapor deposition (CVD) method.[5] Mixed WO_3 (5 mg) and NaBr (0.5 mg) powders are placed inside an alumina boat, and a piece of clean SiO_2/Si wafer is placed on top of the alumina boat with its polished side facing down, which serves as the growth substrate. The alumina boat is then loaded in the center of the quartz tube, and another alumina boat containing S powder (400 mg) is placed at the upstream of the tube. During the synthesis reaction, the tube is heated up to 825 °C and held for 15 min, and the S powder is

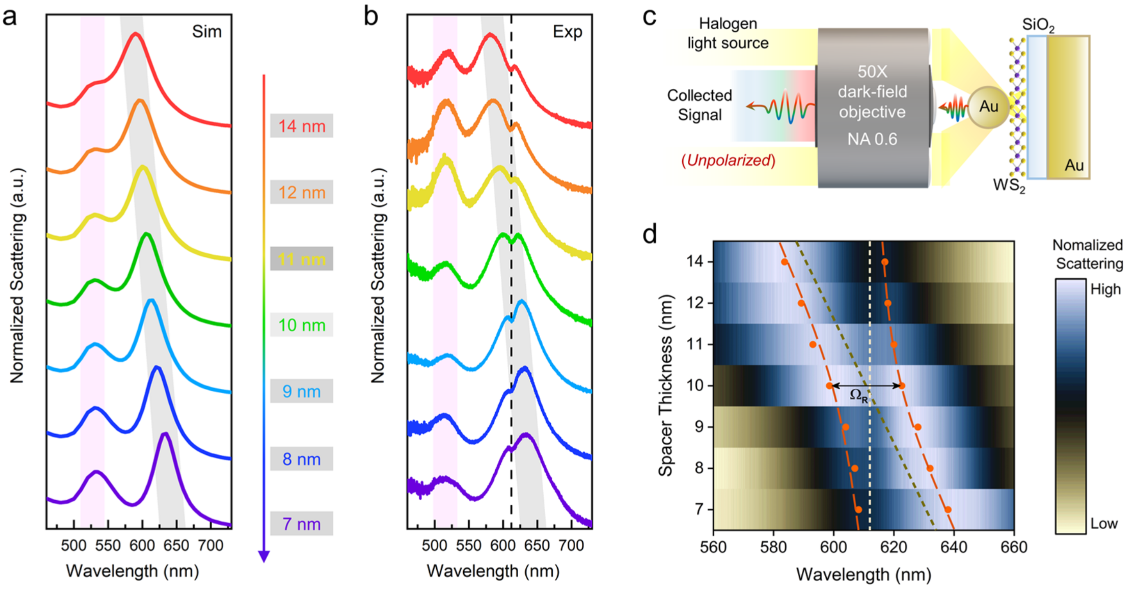

Figure 2. (a) Simulated scattering spectra of a 100 nm AuNS on mirror cavity as a function of SiO_2 spacer thickness. The arrow in red to purple indicates the spacer thickness from 14 to 7 nm. (b) Measured scattering spectra of such a NSoM cavity coupled with monolayer WS_2 as a function of SiO_2 spacer thickness. The black dashed line denotes the WS_2 bright exciton wavelength at 612 nm. (c) Schematic of the optical setup for measuring the spectra in panel (b). The excitation/illumination angles are ∼44−52° from the dark-field objective. A numerical aperture (NA) of 0.6 is also used in simulating the spectra in panel (a) to match the experimental condition. (d) Mapping of the spacer-thickness-dependent scattering spectra in panel (b), showing an anti-crossing behavior (orange dashed curves). The orange dots highlight the peaks extracted from each spectrum. The dip labeled by the white dashed line is from the WS_2 bright exciton. The tilted dark olive dashed line shows the simulated dispersion of the cavity mode S_{11}. The vacuum Rabi splitting Ω_R (85.65 meV) is also highlighted.

heated up simultaneously to 220 °C using a heating belt. Ar (100 sccm) is used as the carrier gas. After the synthesis process, the furnace is cooled down naturally.

Fabrication of Nanosphere-on-Mirror Samples. The gold mirror is fabricated by depositing a 5 nm/100 nm Cr/Au film on a glass substrate by an e-beam evaporator (Kurt J. Lesker PVD75), with a deposition rate of 0.2 Å/s and vacuum under 10^{-5} torr. Then, the silica spacers with different thicknesses are deposited using the same machine. The deposition rate is controlled at 0.1 Å/s. Before the deposition, the glass substrate is cleaned by sonication in acetone, isopropanol, and DI water for 10 min in sequence and blown dry in a nitrogen stream. The thickness of the silica spacer is finally measured with an ellipsometer (J.A. Wollam M2000) and an atomic force microscope (Park Systems NX10), as shown in Figure S1f.

CVD-grown monolayer WS_2 flakes are transferred onto the spacer by a classic PMMA-based wet-transfer process. PMMA (MicroChem 950PMMA A4) is spin-coated on the SiO_2/Si wafer with CVD-grown WS_2 flakes and baked on a hotplate. Then, the PMMA layer with WS_2 is detached by etching the SiO_2 layer in HF solution, washed with DI water two times, attached to the target substrate, dried in vacuum, annealed at 110 °C, and finally removed with acetone.

Finally, 100 nm ultra-uniform gold nanospheres (nanoComposix AUXU100) are drop-cast on the sample by dropping a 50 μL colloidal suspension, which is prepared by diluting the original solution 10 times in ethanol. After total evaporation of the solvent in the droplet, the sample is rinsed with isopropanol and blown dry with nitrogen to remove absorbed surfactants.

Optical Setup and Measurements. An upright microscope (Nikon Ni-E) and a monochromator (Andor Kymera 328i) with an EMCCD (Andor Newton DU970P) are used for the experiments. For standard backward scattering measurements, a halogen lamp is employed as a center-symmetric oblique incident light source through the dark-filed objective (Nikon TU Plan BD ELWD 50×, NA 0.6 WD 11). The incidence angle ranges from 46.8 to 52.9°. For excitation-angle-resolved scattering measurements, a supercontinuum laser (NKT Photonics SuperK Fianium FIU-15) is employed as the white light source. A long-working-distance objective (Nikon TU Plan EPI ELWD 50×, NA 0.5 WD 11) is used to collect the backward scattering signal.

■ RESULTS AND DISCUSSION

Spacer-Thickness- and Excitation-Angle-Dependent Cavity Modes. The NSoM-WS_2 hybrid system under study is shown in Figure 1a. Large-area and high-quality monolayer WS_2 flakes are sandwiched between a 100 nm gold nanosphere (AuNS) and a SiO_2-spacer-covered gold mirror. Detailed sample characterizations can be found in Supporting Information (SI) Section S1 and Figure S1. The commercial AuNSs that we use are decorated with poly(ethylene glycol)-carboxyl and do not show a measurable polymer shell. A circular facet of 47.5 nm diameter at the bottom of AuNS (See Figure 1c) is considered for the best match between all of the simulated and measured spectra.[32]

To start with, we study the applicable modes in NSoM cavities and their tunability. Note that the resonance wavelengths of the bright and dark excitons in monolayer WS_2 are ∼612 and 630 nm, respectively,[24,40] and the material and size/thickness of the nanosphere/spacer are designed accordingly for the spectral overlap.[31,36−38] Figure 1b shows the simulated total scattering efficiency of such a well-designed NSoM cavity with a SiO_2 spacer of 9 nm thickness. The excitation-angle dependence is evaluated by introducing transverse magnetic (TM)-polarized incident light,[36] consid-

https://doi.org/10.1021/acs.jpcc.3c01019
J. Phys. Chem. C 2023, 127, 9105−9112

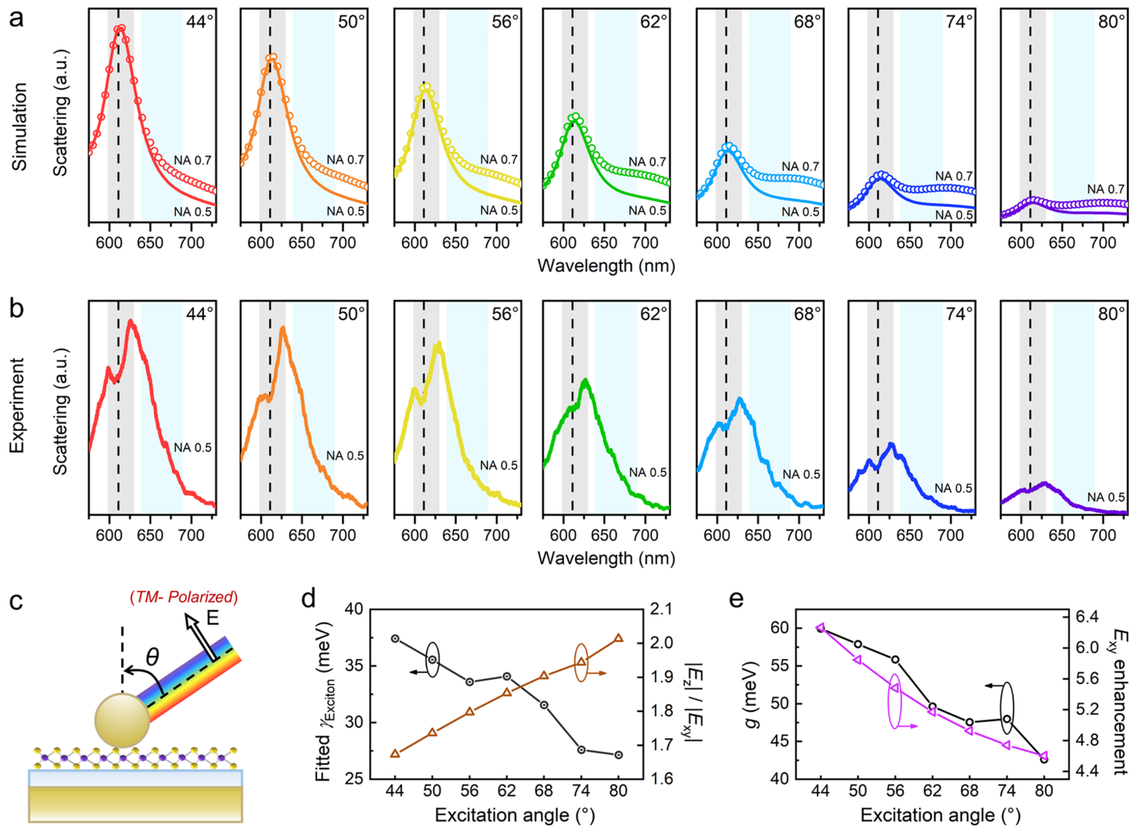

Figure 3. (a) Simulated scattering spectra of a 100 nm AuNS on mirror cavity as a function of excitation angle. The SiO_2 spacer thickness is 9 nm. Numerical apertures (NA) of 0.5 and 0.7 are both evaluated to better identify the out-of-plane cavity mode at longer wavelengths. (b) Measured scattering spectra of such a NSoM cavity coupled with monolayer WS_2 as a function of excitation angle. The black dashed line denotes the WS_2 bright exciton wavelength at 612 nm. In both panels (a) and (b), the excitation light is TM-polarized and from a supercontinuum laser. (c) Schematic of the optical setup. An objective with a NA of 0.5 and a minimum θ of 44° is applied to ensure that only scattering signals are collected. θ is the excitation angle that can be tuned. (d) Fitted exciton linewidth $\gamma_{exciton}$ from measured spectra in panel (b) and simulated ratio of the out-of-plane E_z field magnitude at 630 nm to the in-plane E_{xy} field magnitude at 612 nm at the WS_2 monolayer plane as a function of excitation angle. (e) Fitted coupling strength g for the bright exciton from measured spectra in panel (b) and simulated in-plane E_{xy} field enhancement at 612 nm at the WS_2 monolayer plane as a function of excitation angle.

ering the rotational symmetry of AuNSs. The typical spectra under normal incidence and oblique incidence at 56° are plotted in dashed-dotted and solid lines for comparison. A longer-wavelength mode highlighted by the blue-shaded area is only accessible under oblique incidence, while the areas shaded in pink and gray highlight two modes dominant at normal incidence. We label them as an antenna mode l_{01} (blue) and waveguide modes S_{11} (gray) and S_{12} (pink) based on their mode profiles in Figure 1c,d, in agreement with the literature.[31,36−38] As illustrated in Figure 1c, S_{11} mode is defined by the field distributions at the AuNS−spacer interface and shows an in-plane dipole moment in the gap. S_{12} mode is the higher-order mode featuring a quadrupole in the AuNS (Figure 1c) but with a weaker local E-field intensity (Figure 1d). In contrast, the l_{01} mode possesses an out-of-plane dipole moment (Figure 1c). Therefore, S_{11} and l_{01} modes are chosen to couple with the bright and dark excitons in monolayer WS_2, respectively.

In addition, the resonance wavelength of S_{11} mode can be tuned by choosing different spacer thicknesses, i.e., a blue shift for an increasing spacer thickness and vice versa, as shown in Figure 2a.[19,28] Such tunability helps to investigate the SC of bright excitons and cavity plasmons, which will be discussed in the next section. Moreover, both S_{11} and l_{01} modes can be tuned in mode amplitude with different excitation angles, and the l_{01} mode is especially sensitive, as shown in Figure 3a. This is determined by the z-direction projection of the incident E-fields. Tunable couplings with both dark and bright excitons will be demonstrated based on this concept in the last section.

Strong Coupling with Bright Excitons in Monolayer WS_2. Experimental demonstrations of the SC between bright excitons and S_{11} mode in the scattering spectra of NSoM-WS_2 hybrids with different spacer thicknesses are shown in Figure 2b. Unpolarized and center-symmetric incident light is applied, and the optical setup is illustrated in Figure 2c. It is worth mentioning that a numerical aperture (NA) of 0.6 (not the total scattering) is considered in the simulations for Figure 2a to mimic the experimental condition. More details are in SI Section S2.

We observe a nearly perfect match in mode dispersion between the simulations and experiments—when the spacer thickness decreases from 14 to 7 nm, S_{11} mode red-shifts from 590 to 635 nm. Such a good match is enabled by the relatively accurate tunability in sweeping the spacer thickness, in contrast to the poorer control in sweeping the AuNS size.[32] Besides, the spacer-thickness-dependent S_{11} mode shift is accompanied by negligible changes in mode intensity and linewidth,[19,28] which ensures a consistent dip at the bright exciton wavelength in Figure 2b and a robust anti-crossing feature of polaritons, as plotted in Figure 2d.

https://doi.org/10.1021/acs.jpcc.3c01019
J. Phys. Chem. C 2023, 127, 9105−9112

Table 1. Coupling Strengths of NSoM-WS_2 Hybrids with Different SiO_2 Spacer Thicknesses[a]

spacer thickness (nm)	14	12	11	10	9	8	7
$(\gamma_{cavity} + \gamma_{exciton})/2$ (meV)	72.05	70.42	73.98	69.58	64.16	61.54	68.28
$\sqrt{((\gamma_{cavity})^2 + (\gamma_{exciton})^2)/2}$ (meV)	79.99	77.93	82.70	76.99	70.47	67.80	76.78
$2g$ (meV)	120.1	119.9	99.26	102.6	100.9	98.42	99.26

[a]All of the linewidths are defined in half-width at half-maximum (HWHM).

Table 2. Mode Linewidths and Coupling Strengths of the NSoM-WS_2 Hybrid with a 9 nm Thick SiO_2 Spacer for Different Excitation Angles[a,b]

excitation angle (°)	44	50	56	62	68	74	80
$\gamma_{exciton}$ -Fano (meV)	37.24	35.21	34.00	34.59	31.97	27.60	27.22
$\gamma_{exciton}$ -CMT (meV)	37.62	35.92	33.18	33.59	31.14	27.59	27.05
γ_{cavity} (meV)	91.85	82.04	84.52	85.64	91.18	89.93	95.57
$(\gamma_{cavity} + \gamma_{exciton})/2$ (meV)	64.64	58.80	59.06	59.86	61.37	58.76	61.35
$\sqrt{((\gamma_{cavity})^2 + (\gamma_{exciton})^2)/2}$ (meV)	70.13	63.23	64.31	65.18	68.22	66.52	70.25
$2g$ (meV)	119.9	115.8	111.7	99.26	95.12	95.94	85.20

[a]All of the linewidths are defined in HWHM. [b]$\gamma_{exciton} = (\gamma_{cavity}{}^{-Fano} + \gamma_{exciton}{}^{-CMT})/2$.

In order to explicitly confirm the SC nature, we further fit the spectra in Figure 2b with CMT (See SI Section S3 and Figure S2). Due to the spectral mismatch between the bright exciton and S_{12} mode, only S_{11} mode is accounted in coupling, but both of them are considered in the fittings (See SI Section S4). The fitted coupling strengths g are listed in Table 1. Two thresholds for determining the SC regime,

$$2g > (\gamma_{cavity} + \gamma_{exciton})/2 \tag{1}$$

$$2g > \sqrt{((\gamma_{cavity})^2 + (\gamma_{exciton})^2)/2} \tag{2}$$

are both well reached, proving the nonvanishing Rabi splitting. γ_{cavity} and $\gamma_{exciton}$ are the linewidths of the cavity mode S_{11} and bright excitons, which are double-checked by Fano fittings in Figure S3. All of the fitted parameters can be found in Table S1. Please note that NSoM cavities with a 7 to 14 nm SiO_2 spacer should provide similar field enhancement at the bright exciton wavelength (612 nm) at the WS_2 monolayer plane, according to the simulated values in Figure S7. The difference in coupling strengths can be attributed to the variation of oscillator strengths in different WS_2 flakes, which is commonly observed in CVD-grown TMD monolayers.[42,43] Meanwhile, an averaged g = ∼53 meV gives us a vacuum Rabi splitting $\Omega_R = 2\sqrt{g^2 - (\gamma_{cavity} - \gamma_{exciton})^2/4} = \sim 84\ \text{meV}$, in agreement with the observed Ω_R = 85.65 meV in Figure 2d.

Tunable Bright Exciton Linewidth Mediated by Dark-Exciton−Photon Couplings. Based on the SC of bright-exciton−photon hybrids, we then demonstrate the tunable couplings with both bright and dark excitons and how the dark hybrid state influences the coherent dynamics of bright states, as shown in Figure 3b, through excitation-angle (θ)-resolved scattering spectra. Again, due to the rotational symmetry of AuNSs, TM-polarized incident light is applied to maximize the excitation-angle-sensitive mode tunability,[36] as illustrated in Figure 3c. An optimal sample with a 9 nm thick spacer is studied to ensure the good spectral match between the l_{01} mode and dark exciton in monolayer WS_2. A robust response of the NSoM cavity under excitations at different angles is experimentally confirmed, as shown in Figure S11. Note that, unlike the total scattering in Figure 1b, a limited NA can hardly capture the signal from the out-of-plane l_{01} mode in Figures S11 and 3b. Therefore, we simulate the scattering signals collected within a NA of both 0.5 and 0.7 in Figure 3a. The former shows a good agreement with experimental data in both the spectral line shape and decreasing S_{11} mode intensities with an increasing θ, which confirms the consistency between our analysis and the real situation. The latter shows the emerging l_{01} peak at a longer wavelength, which reaches the dark exciton of monolayer WS_2 at ∼630 nm and becomes more and more dominant with the increasing θ (See Figure S4a). It can thus be hypothesized that although a direct measurement is not available, tunable dark-exciton−photon couplings still exist in the near field.

By normalizing the measured spectra in Figure 3b, a clear tendency of a gradually narrowed bright exciton linewidth with the increasing θ is found in Figure S4b, implying a dark-state-mediated coherent dynamics and thus serving as indirect evidence of tunable dark-exciton−photon couplings. Two extra sets of spectra from the 9 nm thick spacer sample, one set of spectra from the 8 nm thick spacer sample, and one set of spectra from the 10 nm thick spacer sample can be found in Figures S12, S8, and S9, respectively, all showing consistent tunability. To discriminate such phenomena, we applied both Fano and CMT fittings on the measured spectra in Figure 3b. The fittings are included in Figures S5 and S6, and the fitted mode linewidths and coupling strengths are listed in Table 2. The results are also shown in Figure 3d,e (the black dots), confirming the narrowed exciton linewidth from 37.5 down to 27.1 meV, together with a decreasing bright exciton coupling strength from 60.0 down to 42.5 meV, when the NSoM-WS_2 hybrid is excited with oblique incidence at angles from 44 to 80°.

The weakened couplings with bright excitons are intuitive since the absolute intensity of S_{11} mode decreases, as shown in Figure 3b, resulting in a suppressed in-plane E-field enhancement at 612 nm (bright exciton wavelength), as presented in Figure 3e (the purple triangles). The field enhancement is numerically simulated, and the details can be found in SI Section S2. As for the narrowed coherent linewidth of bright excitons, it can be explained by the dynamic competition between bright and dark exciton decays.[4,24] The coherent linewidth of bright excitons is strongly influenced by the

https://doi.org/10.1021/acs.jpcc.3c01019
J. Phys. Chem. C 2023, 127, 9105−9112

phonon-assisted decay channels, which is the so-called homogeneous broadening.[4,44] It has been explored that when the enhanced decay of the spin-forbidden dark state is dominant over the bright exciton decays (including both radiative and phonon-assisted nonradiative ones), the homogeneous broadening effect can be significantly suppressed.[24] In our system, the bright/dark-exciton−photon couplings should both include the Purcell effect that enhances the spontaneous decay rates, and meanwhile, they are separately determined by the in-plane and out-of-plane *E*-fields, matching the corresponding dipole moments. Therefore, we simulate the *E*-fields at the position of WS_2 monolayer and plot the ratio of the out-of-plane E_z field magnitude at 630 nm (dark exciton) to the in-plane E_{xy} field magnitude at 612 nm (bright exciton) in Figure 3d (the brown triangles) as a function of excitation angle. The results confirm our assumptions. As the E_z field (l_{01} mode) becomes more and more dominant, the homogeneous broadening of bright excitons is increasingly suppressed. Finally, this results in the narrowed linewidth and dark-state-mediated tunable modulation of the bright-exciton−polaritons under SC. We notice that the thresholds in eqs 1 and 2 are always well reached for all of the excitation angles (See Table 2), and the bright-exciton−photon hybrids maintain at the SC regime.

CONCLUSIONS

In conclusion, we study the dependence of plasmonic modes in a gold NSoM cavity on the spacer thickness and excitation angle and use them as a platform for tunable couplings with both bright and dark excitons in monolayer TMDs. The waveguide mode S_{11} produces enhanced in-plane *E*-fields at the bright exciton wavelength and supports exciton−plasmon SC with a coupling strength of up to 60 meV at room temperature. The out-of-plane antenna mode l_{01}, overlapping the dark exciton wavelength, shows a decent sensitivity to the excitation angle, giving rise to a novel design dimension for tunable couplings with spin-forbidden dark states. By increasing the excitation angle, we dynamically enlarge the relative contribution from the l_{01} mode coupled with dark excitons and suppress the S_{11} mode coupled with bright states. This not only undermines the bright-exciton−photon coupling strength but also makes the dark exciton decay more dominant over the bright ones, leading to a narrowed bright exciton linewidth. Our demonstration shows dark-state-mediated tunable modulation of the bright-exciton−polaritons under SC, shedding light on the mystery of multiparticle interactions in TMD-based QED. Our findings may inspire new research interests in tunable optical devices and chemistry engineering based on dark excitons as well as in the fundamental study of bright/dark hybridized polaritons in NSoM-TMD cavities.

ASSOCIATED CONTENT

Data Availability Statement

All of the data needed to evaluate the conclusions in the paper are present in the main text or the supporting information. The materials that support the findings of this study are available from the corresponding author upon reasonable request.

Supporting Information

The Supporting Information is available free of charge at https://pubs.acs.org/doi/10.1021/acs.jpcc.3c01019.

Characterization of the samples, COMSOL simulations, Fano and coupled-mode-theory (CMT) fittings, and supplementary angle-resolved scattering spectra (PDF)

AUTHOR INFORMATION

Corresponding Author

Yuebing Zheng − *Walker Department of Mechanical Engineering and Texas Materials Institute, The University of Texas at Austin, Austin, Texas 78712, United States;* orcid.org/0000-0002-9168-9477; Email: zheng@austin.utexas.edu

Authors

Jie Fang − *Walker Department of Mechanical Engineering and Texas Materials Institute, The University of Texas at Austin, Austin, Texas 78712, United States;* orcid.org/0000-0002-0793-9323

Suichu Huang − *Walker Department of Mechanical Engineering and Texas Materials Institute, The University of Texas at Austin, Austin, Texas 78712, United States; Key Laboratory of Micro-Systems and Micro-Structures Manufacturing of Ministry of Education and School of Mechatronics Engineering, Harbin Institute of Technology, Harbin 15001, China*

Kan Yao − *Walker Department of Mechanical Engineering and Texas Materials Institute, The University of Texas at Austin, Austin, Texas 78712, United States;* orcid.org/0000-0002-9144-2618

Tianyi Zhang − *Department of Materials Science and Engineering, Department of Physics, Department of Chemistry and Center for 2-Dimensional and Layered Materials, The Pennsylvania State University, University Park, Pennsylvania 16802, United States; Department of Electrical Engineering and Computer Science, Massachusetts Institute of Technology, Cambridge, Massachusetts 02139, United States*

Mauricio Terrones − *Department of Materials Science and Engineering, Department of Physics, Department of Chemistry and Center for 2-Dimensional and Layered Materials, The Pennsylvania State University, University Park, Pennsylvania 16802, United States;* orcid.org/0000-0003-0010-2851

Wentao Huang − *Key Laboratory of Micro-Systems and Micro-Structures Manufacturing of Ministry of Education and School of Mechatronics Engineering, Harbin Institute of Technology, Harbin 15001, China*

Yunlu Pan − *Key Laboratory of Micro-Systems and Micro-Structures Manufacturing of Ministry of Education and School of Mechatronics Engineering, Harbin Institute of Technology, Harbin 15001, China;* orcid.org/0000-0003-1836-7751

Complete contact information is available at: https://pubs.acs.org/10.1021/acs.jpcc.3c01019

Author Contributions

[⊥]J.F., S.H., and K.Y. contributed equally to this work. J.F. conceived the idea, designed the experiments, and conducted spectra fittings. S.H. and J.F. performed the optical measurements and data analysis with the assistance of K.Y. K.Y., J.F., and S.H. conducted the optical simulations. T.Z. and M.T. prepared and transferred the monolayer WS_2. J.F. and K.Y. fabricated the samples. Y.Z. supervised the project. All authors are involved in discussing the results and writing the manuscript.

Notes

The authors declare no competing financial interest.

■ ACKNOWLEDGMENTS

J.F., S.H., and K.Y. thank Huaizhi Li for his assistance during the fabrication of SiO_2 spacers. J.F., K.Y., and Y.Z. acknowledge the financial support of the National Science Foundation (NSF-ECCS-2001650) and the Portuguese Science and Technology FDN (LOA 028 Zheng). S.H., W.H., and Y.P. acknowledge the financial support of National Natural Science Foundation of China (Grant No. 51975145). T.Z and M.T. thank the Air Force Office of Scientific Research through grant No. FA9550-18-1-0072.

■ REFERENCES

(1) Wang, Q. H.; Kalantar-Zadeh, K.; Kis, A.; Coleman, J. N.; Strano, M. S. Electronics and Optoelectronics of Two-Dimensional Transition Metal Dichalcogenides. *Nat. Nanotechnol.* **2012**, *7*, 699−712.

(2) Hu, H.; Zavabeti, A.; Quan, H.; Zhu, W.; Wei, H.; Chen, D.; Ou, J. Z. Recent Advances in Two-Dimensional Transition Metal Dichalcogenides for Biological Sensing. *Biosens. Bioelectron.* **2019**, *142*, No. 111573.

(3) Li, L.; Shao, L.; Liu, X.; Gao, A.; Wang, H.; Zheng, B.; Hou, G.; Shehzad, K.; Yu, L.; Miao, F.; et al. Room-Temperature Valleytronic Transistor. *Nat. Nanotechnol.* **2020**, *15*, 743−749.

(4) Fang, J.; Yao, K.; Zhang, T.; Wang, M.; Jiang, T.; Huang, S.; Korgel, B. A.; Terrones, M.; Alù, A.; Zheng, Y. Room-Temperature Observation of Near-Intrinsic Exciton Linewidth in Monolayer WS_2. *Adv. Mater.* **2022**, *34*, No. 2270115.

(5) Fang, J.; Wang, M.; Yao, K.; Zhang, T.; Krasnok, A.; Jiang, T.; Choi, J.; Kahn, E.; Korgel, B. A.; Terrones, M.; et al. Directional Modulation of Exciton Emission Using Single Dielectric Nanospheres. *Adv. Mater.* **2021**, *33*, No. 2007236.

(6) Guan, J.; Park, J. E.; Deng, S.; Tan, M. J. H.; Hu, J.; Odom, T. W. Light-Matter Interactions in Hybrid Material Metasurfaces. *Chem. Rev.* **2022**, *122*, 15177−15203.

(7) Zheng, D.; Zhang, S.; Deng, Q.; Kang, M.; Nordlander, P.; Xu, H. Manipulating Coherent Plasmon-Exciton Interaction in a Single Silver Nanorod on Monolayer WSe_2. *Nano Lett.* **2017**, *17*, 3809−3814.

(8) Wang, S.; Li, S.; Chervy, T.; Shalabney, A.; Azzini, S.; Orgiu, E.; Hutchison, J. A.; Genet, C.; Samorì, P.; Ebbesen, T. W. Coherent Coupling of WS_2 Monolayers with Metallic Photonic Nanostructures at Room Temperature. *Nano Lett.* **2016**, *16*, 4368−4374.

(9) Liu, W.; Lee, B.; Naylor, C. H.; Ee, H. S.; Park, J.; Johnson, A. T. C.; Agarwal, R. Strong Exciton-Plasmon Coupling in MoS_2 Coupled with Plasmonic Lattice. *Nano Lett.* **2016**, *16*, 1262−1269.

(10) Ribeiro, R. F.; Martínez-Martínez, L. A.; Du, M.; Campos-Gonzalez-Angulo, J.; Yuen-Zhou, J. Polariton Chemistry: Controlling Molecular Dynamics with Optical Cavities. *Chem. Sci.* **2018**, *9*, 6325−6339.

(11) Kavokin, A.; Liew, T. C. H.; Schneider, C.; Lagoudakis, P. G.; Klembt, S.; Hoefling, S. Polariton Condensates for Classical and Quantum Computing. *Nat. Rev. Phys.* **2022**, *4*, 435−451.

(12) Li, J.; Yao, K.; Huang, Y.; Fang, J.; Kollipara, P. S.; Fan, D. E.; Zheng, Y. Tunable Strong Coupling in Transition Metal Dichalcogenide Nanowires. *Adv. Mater.* **2022**, *34*, No. 2200656.

(13) Chakraborty, B.; Gu, J.; Sun, Z.; Khatoniar, M.; Bushati, R.; Boehmke, A. L.; Koots, R.; Menon, V. M. Control of Strong Light-Matter Interaction in Monolayer WS_2 through Electric Field Gating. *Nano Lett.* **2018**, *18*, 6455−6460.

(14) Dibos, A. M.; Zhou, Y.; Jauregui, L. A.; Scuri, G.; Wild, D. S.; High, A. A.; Taniguchi, T.; Watanabe, K.; Lukin, M. D.; Kim, P.; Park, H. Electrically Tunable Exciton-Plasmon Coupling in a WSe_2 Monolayer Embedded in a Plasmonic Crystal Cavity. *Nano Lett.* **2019**, *19*, 3543−3547.

(15) Munkhbat, B.; Baranov, D. G.; Bisht, A.; Hoque, M. A.; Karpiak, B.; Dash, S. P.; Shegai, T. Electrical Control of Hybrid Monolayer Tungsten Disulfide-Plasmonic Nanoantenna Light-Matter States at Cryogenic and Room Temperatures. *ACS Nano* **2020**, *14*, 1196−1206.

(16) Wang, M.; Krasnok, A.; Zhang, T.; Scarabelli, L.; Liu, H.; Wu, Z.; Liz-Marzán, L. M.; Terrones, M.; Alù, A.; Zheng, Y. Tunable Fano Resonance and Plasmon−Exciton Coupling in Single Au Nanotriangles on Monolayer WS_2 at Room Temperature. *Adv. Mater.* **2018**, *30*, No. 1705779.

(17) Lepeshov, S.; Wang, M.; Krasnok, A.; Kotov, O.; Zhang, T.; Liu, H.; Jiang, T.; Korgel, B.; Terrones, M.; Zheng, Y.; Alú, A. Tunable Resonance Coupling in Single Si Nanoparticle-Monolayer WS_2 Structures. *ACS Appl. Mater. Interfaces* **2018**, *10*, 16690−16697.

(18) Dufferwiel, S.; Schwarz, S.; Withers, F.; Trichet, A. A. P.; Li, F.; Sich, M.; Del Pozo-Zamudio, O.; Clark, C.; Nalitov, A.; Solnyshkov, D. D.; et al. Exciton-Polaritons in van Der Waals Heterostructures Embedded in Tunable Microcavities. *Nat. Commun.* **2015**, *6*, No. 8579.

(19) Kleemann, M. E.; Chikkaraddy, R.; Alexeev, E. M.; Kos, D.; Carnegie, C.; Deacon, W.; De Pury, A. C.; Große, C.; De Nijs, B.; Mertens, J.; et al. Strong-Coupling of WSe_2 in Ultra-Compact Plasmonic Nanocavities at Room Temperature. *Nat. Commun.* **2017**, *8*, No. 1296.

(20) Wang, G.; Robert, C.; Glazov, M. M.; Cadiz, F.; Courtade, E.; Amand, T.; Lagarde, D.; Taniguchi, T.; Watanabe, K.; Urbaszek, B.; Marie, X. In-Plane Propagation of Light in Transition Metal Dichalcogenide Monolayers: Optical Selection Rules. *Phys. Rev. Lett.* **2017**, *119*, No. 047401.

(21) Arora, A.; Dixit, T.; Kumar, K. V. A.; Krishnan, S.; Ganapathi, K. L.; Krishnan, A.; Nayak, P. K.; Rao, M. S. R. Plasmon Induced Brightening of Dark Exciton in Monolayer WSe_2 for Quantum Optoelectronics. *Appl. Phys. Lett.* **2019**, *114*, No. 201101.

(22) Lo, T. W.; Chen, X.; Zhang, Z.; Zhang, Q.; Leung, C. W.; Zayats, A. V.; Lei, D. Plasmonic Nanocavity Induced Coupling and Boost of Dark Excitons in Monolayer WSe_2 at Room Temperature. *Nano Lett.* **2022**, *22*, 1915−1921.

(23) Park, K. D.; Jiang, T.; Clark, G.; Xu, X.; Raschke, M. B. Radiative Control of Dark Excitons at Room Temperature by Nano-Optical Antenna-Tip Purcell Effect. *Nat. Nanotechnol.* **2018**, *13*, 59−64.

(24) Wang, M.; Wu, Z.; Krasnok, A.; Zhang, T.; Liu, M.; Liu, H.; Scarabelli, L.; Fang, J.; Liz-Marzán, L. M.; Terrones, M.; et al. Dark-Exciton-Mediated Fano Resonance from a Single Gold Nanostructure on Monolayer WS_2 at Room Temperature. *Small* **2019**, *15*, No. 1900982.

(25) Ferreira, B.; Rosati, R.; Fitzgerald, J.; Malic, E. Signatures of Dark Excitons in Exciton-Polariton Optics of Transition Metal Dichalcogenides. *2D Mater.* **2022**, *10*, No. 015012.

(26) Lo, T. W.; Zhang, Q.; Qiu, M.; Guo, X.; Meng, Y.; Zhu, Y.; Xiao, J. J.; Jin, W.; Leung, C. W.; Lei, D. Thermal Redistribution of Exciton Population in Monolayer Transition Metal Dichalcogenides Probed with Plasmon-Exciton Coupling Spectroscopy. *ACS Photonics* **2019**, *6*, 411−421.

(27) Latini, S.; Ronca, E.; De Giovannini, U.; Hübener, H.; Rubio, A. Cavity Control of Excitons in Two-Dimensional Materials. *Nano Lett.* **2019**, *19*, 3473−3479.

(28) Lassiter, J. B.; McGuire, F.; Mock, J. J.; Ciracì, C.; Hill, R. T.; Wiley, B. J.; Chilkoti, A.; Smith, D. R. Plasmonic Waveguide Modes of Film-Coupled Metallic Nanocubes. *Nano Lett.* **2013**, *13*, 5866−5872.

(29) Li, G. C.; Zhang, Q.; Maier, S. A.; Lei, D. Plasmonic Particle-on-Film Nanocavities: A Versatile Platform for Plasmon-Enhanced Spectroscopy and Photochemistry. *Nanophotonics* **2018**, *7*, 1865−1889.

(30) Li, Y.; Li, D.; Chi, C.; Huang, B. Achieving Strong Field Enhancement and Light Absorption Simultaneously with Plasmonic

Nanoantennas Exploiting Film-Coupled Triangular Nanodisks. *J. Phys. Chem. C* **2017**, *121*, 16481−16490.
(31) Chen, S.; Zhang, Y.; Shih, T.-M.; Yang, W.; Hu, S.; Hu, X.; Li, J.; Ren, B.; Mao, B.; Yang, Z.; Tian, Z. Plasmon-Induced Magnetic Resonance Enhanced Raman Spectroscopy. *Nano Lett.* **2018**, *18*, 2209−2216.
(32) Huh, J. H.; Lee, J.; Lee, S. Comparative Study of Plasmonic Resonances between the Roundest and Randomly Faceted Au Nanoparticles-on-Mirror Cavities. *ACS Photonics* **2018**, *5*, 413−421.
(33) Akselrod, G. M.; Argyropoulos, C.; Hoang, T. B.; Ciracì, C.; Fang, C.; Huang, J.; Smith, D. R.; Mikkelsen, M. H. Probing the Mechanisms of Large Purcell Enhancement in Plasmonic Nanoantennas. *Nat. Photonics* **2014**, *8*, 835−840.
(34) Wang, Z.; Liu, L.; Zhang, D.; Krasavin, A. V.; Zheng, J.; Pan, C.; He, E.; Wang, Z.; Zhong, S.; Li, Z.; et al. Effect of Mirror Quality on Optical Response of Nanoparticle-on-Mirror Plasmonic Nanocavities. *Adv. Opt. Mater.* **2022**, *11*, No. 2201914.
(35) Yao, K.; Zheng, Y. *Nanophotonics and Machine Learning*; Springer Nature: Cham, Switzerland, 2023.
(36) Hu, H.; Xu, Y.; Hu, Z.; Kang, B.; Zhang, Z.; Sun, J.; Li, Y.; Xu, H. Nanoparticle-on-Mirror Pairs: Building Blocks for Remote Spectroscopies. *Nanophotonics* **2022**, *11*, 5153−5163.
(37) Huang, Y.; Ma, L.; Li, J.; Zhang, Z. Nanoparticle-on-Mirror Cavity Modes for Huge and/or Tunable Plasmonic Field Enhancement. *Nanotechnology* **2017**, *28*, No. 105203.
(38) Tserkezis, C.; Esteban, R.; Sigle, D. O.; Mertens, J.; Herrmann, L. O.; Baumberg, J. J.; Aizpurua, J. Hybridization of Plasmonic Antenna and Cavity Modes: Extreme Optics of Nanoparticle-on-Mirror Nanogaps. *Phys. Rev. A* **2015**, *92*, No. 053811.
(39) Zhang, X. X.; You, Y.; Zhao, S. Y. F.; Heinz, T. F. Experimental Evidence for Dark Excitons in Monolayer WSe_2. *Phys. Rev. Lett.* **2015**, *115*, No. 257403.
(40) Molas, M. R.; Faugeras, C.; Slobodeniuk, A. O.; Nogajewski, K.; Bartos, M.; Basko, D. M.; Potemski, M. Brightening of Dark Excitons in Monolayers of Semiconducting Transition Metal Dichalcogenides. *2D Mater.* **2017**, *4*, No. 021003.
(41) Slobodeniuk, A. O.; Basko, D. M. Spin-Flip Processes and Radiative Decay of Dark Intravalley Excitons in Transition Metal Dichalcogenide Monolayers. *2D Mater.* **2016**, *3*, No. 035009.
(42) Rosenberger, M. R.; Chuang, H.-J.; McCreary, K. M.; Li, C. H.; Jonker, B. T. Electrical Characterization of Discrete Defects and Impact of Defect Density on Photoluminescence in Monolayer WS_2. *ACS Nano* **2018**, *12*, 1793−1800.
(43) Ren, D.-D.; Qin, J.-K.; Li, Y.; Miao, P.; Sun, Z.-Y.; Xu, P.; Zhen, L.; Xu, C.-Y. Photoluminescence inhomogeneity and excitons in CVD-grown monolayer WS_2. *Opt. Mater.* **2018**, *80*, 203−208.
(44) Selig, M.; Berghäuser, G.; Raja, A.; Nagler, P.; Schüller, C.; Heinz, T. F.; Korn, T.; Chernikov, A.; Malic, E.; Knorr, A. Excitonic Linewidth and Coherence Lifetime in Monolayer Transition Metal Dichalcogenides. *Nat. Commun.* **2016**, *7*, No. 13279.